Available online at www.sciencedirect.com
ScienceDirect
ELSEVIER
Nuclear Physics A 783 (2007) 233c–240c
NUCLEAR PHYSICS A

Suppression of Heavy Quarks in Heavy-ion Collisions

Che Ming Ko and Wei Liu

Cyclotron Institute and Physics Department, Texas A&M University
College Station, Texas 77843, USA

Abstract

Heavy quark drag coefficients in a quark-gluon plasma due to three-body elastic scattering have recently been approximately evaluated in the lowest order in QCD. For both charm and bottom quarks, their values are found to be comparable to those from two-body elastic scattering. In the Fokker-Planck approach based on a schematic expanding fireball model, its effect on the transverse momentum spectra of heavy quarks produced from Au+Au collisions at center of mass energy $\sqrt{s_{NN}} = 200$ has been studied, and the results show that adding contributions from heavy quark three-body scattering to those due to two-body elastic and radiative scattering brings the nuclear modification factor for electrons from heavy meson decays closer to available experimental data.

1 Introduction

Although heavy mesons produced in heavy ion collisions at the Relativistic Heavy Ion Collider (RHIC) have not been reconstructed from their decay product, the electrons from their semi-leptonic decays have, however, been identified. These electrons were found to have an appreciable elliptic flow [1,2] as well as a large suppression at high transverse momenta [3,4]. Both observations are consistent with the prediction of Ref.[5] based on the assumption that charm quarks are thermalized in the produced quark-gluon plasma, developing thus a similar elliptic flow to that of light quarks and a softer transverse momentum spectrum than their initial power-low spectrum. In the Fokker-Planck approach [6] as well as the transport model [7,8], it has been shown

⋆ Supported in part by the US National Science Foundation under Grant No. PHY-0457265 and the Welch Foundation under Grant No. A-1358.

0375-9474/$ – see front matter
doi:10.1016/j.nuclphysa.2006.11.079

that to explain the experimental observations requires a charm quark two-body elastic scattering cross section that is much larger than that given by the perturbative QCD. According to Ref.[9], such a large cross section could be due to the non-perturbative effect of forming colorless resonances between charm quarks and the light quarks in the QGP. The large charm quark two-body elastic scattering cross section could also be considered as an effective one that takes into account two-body radiative scattering of charm quarks. As shown in Refs.[10–12], the latter process leads to an appreciable energy loss for charm quarks in the QGP, although its effect for bottom quarks is small due to their large masses. Whether the radiative energy loss mechanism can explain the observed suppression of electrons from heavy meson decays depends, however, on the spectra of initially produced charm and bottom quarks used in the theoretical calculations [13,14].

Since the density of the partonic matter formed in heavy ion collisions at RHIC is large, ranging from about 1 fm^{-3} near hadronization to more than 10 fm^{-3} during the initial stage, three-body elastic scattering may also contribute to heavy quark energy loss in the QGP. This effect has recently been studied in Ref.[15] and is found to be comparable to that due to two-body elastic scattering [16,17]. In this talk, these results are reported.

2 Heavy quark scattering in QGP

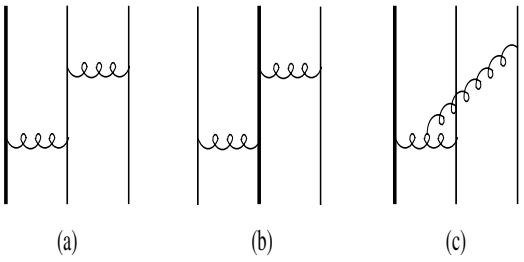

Fig. 1. Topologically different diagrams for heavy quark (thick lines) three-body elastic scattering by quarks and antiquarks (thin lines) with different flavors. Curled lines denote gluons.

Three-body scattering of heavy quarks in the QGP can involve both quarks and gluons. For the processes $Qqq \to Qqq$, $Q\bar{q}\bar{q} \to Q\bar{q}\bar{q}$, and $Qq\bar{q} \to Qq\bar{q}$ with different light quark (q) and antiquark ($\bar{q}$) flavors, there are three topologically different diagrams in the lowest-order QCD as shown in Fig. 1. While diagram (c) corresponds to one diagram, two diagrams are generated from diagram (b), corresponding to either the left or the right gluon (curled line) is first exchanged, and four diagrams are generated from diagram (a) by exchanging the two gluons in all possible ways but keeping only one attached to the heavy quark. To ensure true three-body scattering, the intermediate quark in both

diagrams (a) and (b) of Fig. 1 must be off-shell, and this can be achieved by including its collisional width Γ in the QGP and keeping only the real part of its propagator in evaluating these diagrams.

If the two light quarks or antiquarks in Fig. 1 have same flavor, the number of diagrams is then doubled by interchanging final two light quarks or antiquarks. These exchange diagrams give same contribution as that due to the direct diagrams in Fig. 1. For the process $Qq\bar{q} \to Qq\bar{q}$ with same quark and antiquark flavor, besides diagrams similar to those of Fig. 1, the quark and antiquark can annihilate to a time-like virtual gluon, giving rise to additional five diagrams corresponding to different ways a gluon is exchanged.

For heavy quark three-body elastic scattering involving gluons, the number of allowed diagrams is even larger; i.e., 36 diagrams for the process $Qqg \to Qqg$ or $Q\bar{q}g \to Q\bar{q}g$, and 123 diagrams for the process $Qgg \to Qgg$.

3 Heavy quark drag coefficients in QGP

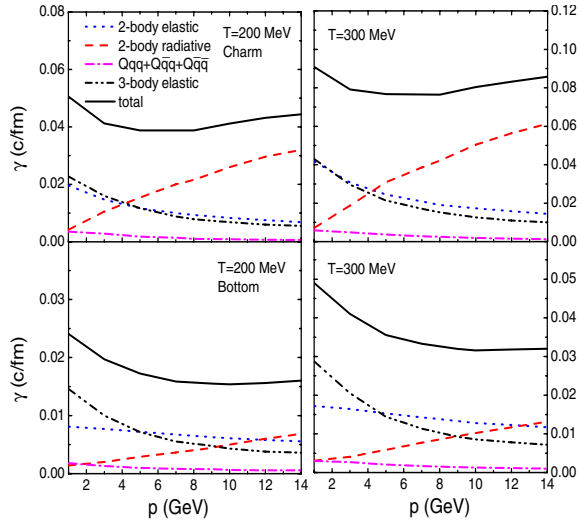

Fig. 2. (Color online) Charm (upper panels) and bottom (lower panels) quark drag coefficients as functions of their momentum in a QGP of temperature $T = 200$ MeV (left panels) or $T = 300$ MeV (right panels).

In the Fokker-Planck approach [18], the momentum degradation of a heavy quark in the QGP depends on its drag coefficient, which is given by the momentum transfer weighted thermal average of the squared transition amplitudes $\overline{|M_i|^2}$, i.e., $\gamma(|\mathbf{p}|, T) = \sum_i \left(\langle \overline{|M_i|^2} \rangle - \langle \overline{|M_i|^2} \mathbf{p} \cdot \mathbf{p}' \rangle / |\mathbf{p}|^2 \right)$, with $\mathbf{p}$ and $\mathbf{p}'$ being, respectively, the momenta of the heavy quark before and after a collision.

In Fig. 2, we show the charm (upper panels) and bottom (lower panels) quark drag coefficients as functions of their momentum in QGP at temperatures $T = 200$ MeV (left panels) and $T = 300$ MeV (right panels). They are obtained by using the QCD coupling $\alpha_s = g^2/4\pi = 0.3$ and including the screening mass $m_D = gT$ for space-like gluons as well as the thermal masses $m_g = \sqrt{3}m_q = m_D/\sqrt{2}$ for time-like gluons and quarks [19]. It is seen that for both charm and bottom quarks the contribution from three-body scattering by light quarks and antiquarks with different flavors (dash-dotted line) is generally smaller than those from two-body elastic (dotted line) and radiative scatterings (dashed line). We note that while the contribution from diagram (a) of Fig. 1 is the largest at high momentum, that from diagram (b) is more important at low momentum, and both are more than one order of magnitude larger than that from diagram (c).

For light quarks or antiquarks with same flavors, the contribution from the annihilation diagrams is found to be small. Neglecting the small interference between these diagrams and the diagrams in Fig. 1 as well as that between the direct and exchange diagrams for scattering by two identical quarks or antiquarks, the contribution from quarks and antiquarks with same flavor is then the same as that from quarks and antiquarks with different flavors. We have not been able to evaluate all the diagrams for heavy quark three-body scattering involving gluons. Instead, we assume that these processes are also dominated by diagrams similar to diagrams (a) and (b) of Fig. 1. In this case, the contribution from $Qgg \to Qgg$ to heavy quark drag coefficients is slightly larger while that from $Qqg \to Qqg$ and $Q\bar{q}g \to Q\bar{q}g$ is about a factor of three larger than that due to scattering by quarks and antiquarks, essentially due to the associated color and flavor factors in these processes. Including these contributions leads to heavy quark drag coefficients due to three-body elastic scattering (dash-dot-dotted line in Fig. 2) that are comparable to those due to two-body elastic scattering. The resulting total drag coefficients for heavy quarks due to both two- and three-body scattering are shown by solid lines in Fig. 2.

4 Heavy quark momentum degradation in QGP

To see the effect of three-body elastic scattering on heavy quark momentum degradation in QGP, we consider central Au+Au collisions at center-of-mass energy $\sqrt{s_{NN}} = 200$ GeV. The initial p_T spectra of charm and bottom quarks at midrapidity are taken to be

$$\frac{dN_c}{d^2p_T} = \frac{19.2[1 + (p_T/6)^2]}{(1 + p_T/3.7)^{12}[1 + \exp(0.9 - 2p_T)]}$$

$$\frac{dN_b}{d^2p_T} = 0.0025\left[1 + (p_T/16)^5\right]\exp(-p_T/1.495), \quad (1)$$

respectively, with p_T in unit of GeV/c. Both are obtained by multiplying the heavy quark p_T spectra from p+p collisions at same energy by the number of binary collisions (~ 960) in Au+Au collisions. For bottom quarks, their p_T spectrum in p+p collisions is taken from the upper limit of the uncertainty band of the pQCD predictions in Ref.[20] as there is no empirical information, while for charm quarks it is determined instead from fitting simultaneously measured p_T spectrum of charmed mesons from d+Au collisions [21] and of electrons from heavy meson decays in p+p collisions. In obtaining the latter, heavy quarks are fragmented to hadrons via the Peterson fragmentation function, $D(z) \propto 1/z[1 - 1/z - \epsilon/(1-z)]^2$, where z is the fraction of heavy quark momentum carried by the formed meson, with ϵ taken to be 0.02 for charm quarks and 0.002 for bottom quarks in order to reproduce the empirical fragmentation functions used in Ref.[20]. These heavy quarks are then distributed in the transverse plane according to that of the binary collision number and their transverse momenta are directed isotropically in the transverse plane.

For the dynamics of formed QGP, we assume that it evolves boost invariantly in the longitudinal direction but with an accelerated transverse expansion. Specifically, its volume expands in the proper time τ according to $V(\tau) = \pi R(\tau)^2\tau$, where $R(\tau) = R_0 + a/2(\tau - \tau_0)^2$ is the transverse radius with an initial value R_0=7 fm, τ_0=0.6 fm is the QGP formation time, and $a = 0.1c^2$/fm is the transverse acceleration [22]. With an initial temperature $T_i = 350$ MeV and using thermal masses for quarks and gluons, this model gives a total transverse energy comparable to that measured in experiments. The time dependence of the temperature is obtained from entropy conservation, and the critical temperature $T_c = 175$ MeV is reached at proper time $\tau_c \sim 5$ fm.

Time evolution of the mean transverse momentum of a heavy quark in the QGP can be obtained from the Fokker-Planck equation, i.e., $d\langle p_T\rangle/dt = -\langle\gamma(p_T, T)p_T\rangle \approx -\gamma_0(\langle p_T\rangle + a\langle p_T\rangle^2)$. Its final mean transverse is determined at the time when it escapes the QGP or when the QGP phase ends. Averaging over the initial spatial and transverse momentum distributions of heavy quarks then gives their final transverse momentum spectra. Heavy quarks are further converted to heavy mesons via fragmentation and subsequently decay to electrons in order to compare with those measured in experiments.

In Fig. 3, we show by solid lines the transverse momentum spectra of heavy quarks. The initial spectra are given in panel (a). For both charm and bottom quarks, their final p_T spectra become softer with the inclusion of more scattering processes: panel (b) for two-body elastic scattering only, panel (c) for both two-body elastic and radiative scatterings, panel (d) for adding also three-body scattering by light quarks and antiquarks with different flavors,

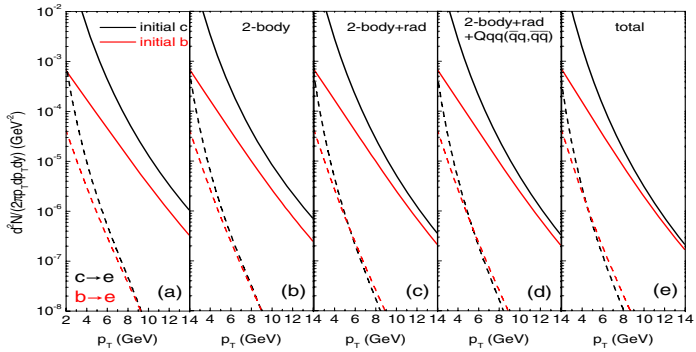

Fig. 3. (Color online) Transverse momentum spectra of heavy quarks (solid lines) and their decay electrons (dashed lines) in central Au+Au collisions at $\sqrt{s_{NN}} = 200$ GeV: (a) initial; (b) after two-body elastic scattering; (c) including also two-body radiative scattering; (d) further including three-body scattering by quarks and antiquarks with different flavors; (e) including other three-body scattering as well.

and panel (e) for further including other three-body scattering processes. Although bottom quarks are negligible at low transverse momentum, they are important at high transverse momentum as a result of their smaller momentum degradation in QGP than charm quarks. The spectra of electrons from resulting heavy mesons are shown by dashed lines in Fig.3, and they are much softer than the spectra of heavy quarks. Because of large bottom quark mass, electrons from their decays become dominant at high p_T.

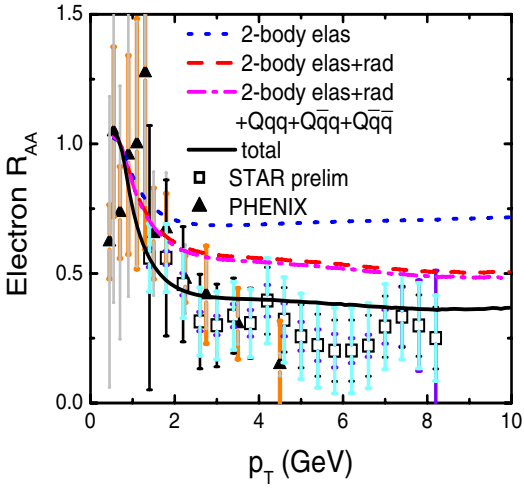

Fig. 4. (Color online) The nuclear modification factor R_{AA} for electrons from heavy quark decays in central Au+Au collisions at $\sqrt{s_{NN}} = 200$ GeV.

The ratio of the electron p_T spectrum from final heavy mesons to that from initially produced ones, defined as the electron nuclear modification factor R_{AA}, is shown in Fig. 4. It is seen that the effect from two-body elastic scattering (dotted line) is as important as that from two-body radiative scattering, similar to that of Ref.[17]. The electron R_{AA} including both contributions (dashed

line) is, however, above the experimental data from the PHENIX collaboration (filled triangles) [3] and the preliminary data from the STAR collaboration (open squares) [4]. Adding the contribution from heavy quark three-body elastic scattering increases heavy quark energy loss, leading to an electron R_{AA} that is much closer to the measured one as shown by the solid line. If we include only heavy quark three-body scattering by light quarks and antiquarks of different flavors, which is more reliably computed in present study, the resulting electron R_{AA} is shown by the dash-dotted line and is essentially similar to that due to two-body elastic and radiative scattering.

5 Summary and discussions

In the lowest-order QCD and including thermal masses of quarks and gluons as well as the screening mass of exchanged gluons, the drag coefficients of heavy quarks in QGP due to their three-body elastic scattering are found to be comparable to those from two-body elastic scattering. Taking the initial charm quark spectrum from empirical measurements and the initial bottom quark spectrum from pQCD, the nuclear modification factor for electrons from heavy meson decays in central Au+Au collisions at $\sqrt{s_{NN}} = 200$ GeV becomes close to the upper error bars of preliminary experimental data if both heavy quark two-body elastic and radiative scattering as well as three-body elastic scattering are included. If the initial bottom quark spectrum is obtained from the lower limit of the uncertainty band of pQCD predictions, which is about a factor of two smaller, the resulting electron R_{AA} is then reduced by about 20%, leading to a better agreement with experimental data. On the other hand, taking the initial charm quark spectrum from the lower limit while the bottom quark spectrum from the upper limit of the uncertainty band in the pQCD predictions increases the electron R_{AA} by about 40%, which is at variance with the experimental data. To understand the measured electron R_{AA} thus requires better information on the initial heavy quark spectra.

The most important heavy quark three-body elastic scattering process involves scattering with a gluon and a light quark or antiquark in the QGP, and this contribution has been evaluated using the assumption that they are dominated by t-channel gluon-exchange diagrams similar to diagrams (a) and (b) of Fig. 1 for three-body scattering by quarks and antiquarks with different flavors. Although this is a valid approximation for the latter process, its validity for the former process remains to be verified. Also, interference terms between charm quark radiative scattering with and without vertex corrections contribute to the same order in QCD coupling, i.e., α_s^4, as three-body elastic scattering and needs to be studied as well.

References

[1] PHENIX Collaboration, S.S. Adler *et al.*, Phys. Rev. C 72 (2005) 024901.

[2] F. Lauer and STAR Collaboration, J. Phys. G 31 (2005) S27.

[3] PHENIX Collaboration, S.S. Adler *et al.*, Phys. Rev. Lett. 96 (2006) 032301.

[4] J. Bielcik and STAR Collaboration, Nucl. Phys. A 774 (2006) 697.

[5] V. Greco, C.M. Ko, and R. Rapp, Phys. Lett. B 595 (2004) 202.

[6] G.D. Moore and D. Teaney, Phys. Rev. C 71 (2005) 064904.

[7] D. Molnar, J. Phys. G 31 (2005) S421.

[8] B. Zhang, L.W. Chen, and C.M. Ko, Phys. Rev. C 72 (2005) 024906; Nucl. Phys. A 774 (2006) 665.

[9] H. van Hees and R. Rapp, Phys. Rev. C 71 (2005) 034907; H. van Hees, V. Greco, and R. Rapp, Phys. Rev. C 73 (2006) 034913.

[10] B.W. Zhang, E.K. Wang, and X.N. Wang, Phys. Rev. Lett. 93 (2004) 072301; Nucl. Phys. A 757 (2005) 493.

[11] N. Armesto, C.A. Salgado, and U.A. Wiedemann, Phys. Rev. D 69 (2004) 114003.

[12] M. Djordjevic, M. Gyulassy, and S. Wicks, Phys. Rev. Lett. 94 (2005) 112301.

[13] M. Djordjevic, M. Gyulassy, R. Vogt, and S. Wicks, Phys. Lett. B 632 (2006) 81.

[14] N. Armesto *et al.*, Phys. Lett. B 637 (2006) 362.

[15] W. Liu and C.M. Ko, nucl-th/0603004.

[16] M.G. Mustafa, Phys. Rev. C 72 (2005) 014905; M.G. Mustafa, D. Pal, D.K. Srivastava, M.H. Thoma, Phys. Lett. B 428 (1998) 234.

[17] S. Wicks, W. Horowitz, M. Djordjevic, and M. Gyulassy, nucl-th/0512076.

[18] B. Svetitsky, Phys. Rev. D 37 (1988) 2484.

[19] J.P. Blaizot and E. Iancu, Phys. Rep. 359 (2002) 355.

[20] M. Cacciari, P. Nason, and R. Vogt, Phys. Rev. Lett. 95 (2005) 122001.

[21] STAR Collaboration, J. Adams *et al.*, Phys. Rev. Lett. 94 (2005) 062301.

[22] L.W. Chen, V. Greco, C.M. Ko, S.H. Lee, and W. Liu, Phys. Lett. B 601 (2004) 34.